PAPER Nr.: 6

PRESSURE FLUCTUATIONS ON ROTOR BLADES GENERATED BY BLADE VOTEX INTERACTION

G. NEUWERTH and R. MÜLLER

TECHNICAL UNIVERSITY OF AACHEN

AACHEN, F.R.G.

TENTH EUROPEAN ROTORCRAFT FORUM

AUGUST 28 – 31, 1984 – THE HAGUE, THE NETHERLANDS

Abstract

During some flight operations of helicopters the main rotor blades pass close or intersect the trailing tip vortices of the main rotor. These Blade-Vortex-Interactions (BVI) generate strong fluctuating blade pressures leading to dynamic structural loads and impulsive noise radiation. Currently, accurate load predictions are limited by the lack of knowledge of the tip vortex structure. Therefore, a special test facility was built to investigate the basic mechanism of BVI: a special delta wing generates two leading edge vortices with a structure measured by a five hole probe. One of these vortices interacts with a rotor which represents the main rotor. The forward flight of the helicopter is simulated by a windtunnel. By this arrangement a better physical understanding of the BVI can be obtained. Additionally, theoretical methods for computing the local unsteady blade pressures can be checked more reliably. The pressure fluctuations are computed by means of a theory which was derived from the unsteady airfoil theory of NAUMANN and YEH. Measured and computed pressure fluctuations are in good agreement.

1. Introduction

The use of helicopters may become severely limited due to the radiated noise generated by the rotor system. Noise regulations which govern the operation of these vehicles may limit their use. Noise has to be treated thoroughly early in the design process. An "acoustic design change" may decrease vehicle performance and must be weighted against other competing factors. Therefore, a fundamental understanding of the aerodynamic noise generation by the rotor system is necessary. The *impulsive noise is the most prominent* of the helicopter noise events. It occurs during special flight conditions as the dominant noise source. At least two different mechanisms are responsible for the impulsive noise: *compressibility effects and blade-vortex interaction* (BVI). Full-scale measurements of BVI noise have been carried out by BOXWELL and SCHMITZ /1/.

In this paper some aerodynamic aspects of the BVI mechanism are analysed. The experimental and theoretical investigations are done at lower rotor tip Mach numbers $M_t \leq 0,52$. *Thus, compressibility effects are* nearly of no consequence. BVI occurs if a main rotor blade interacts with previously generated tip vortices. These vortices are shed from the tips of the blades and pass near to the rotor disk (s. figure 1). Under certain sets of flight conditions, especially during steady descending flight, the vortex path goes through the rotor disk plane; the vortices are cut by the blades leading to strong BVI. Unsteady disturbances which rapidly change the local blade flow field are generated by the vortices. The local angle of attack and the dynamic pressure at the blades yield impulsive changes of air pressures and forces. This effect leads to impulsive noise and structural loads.

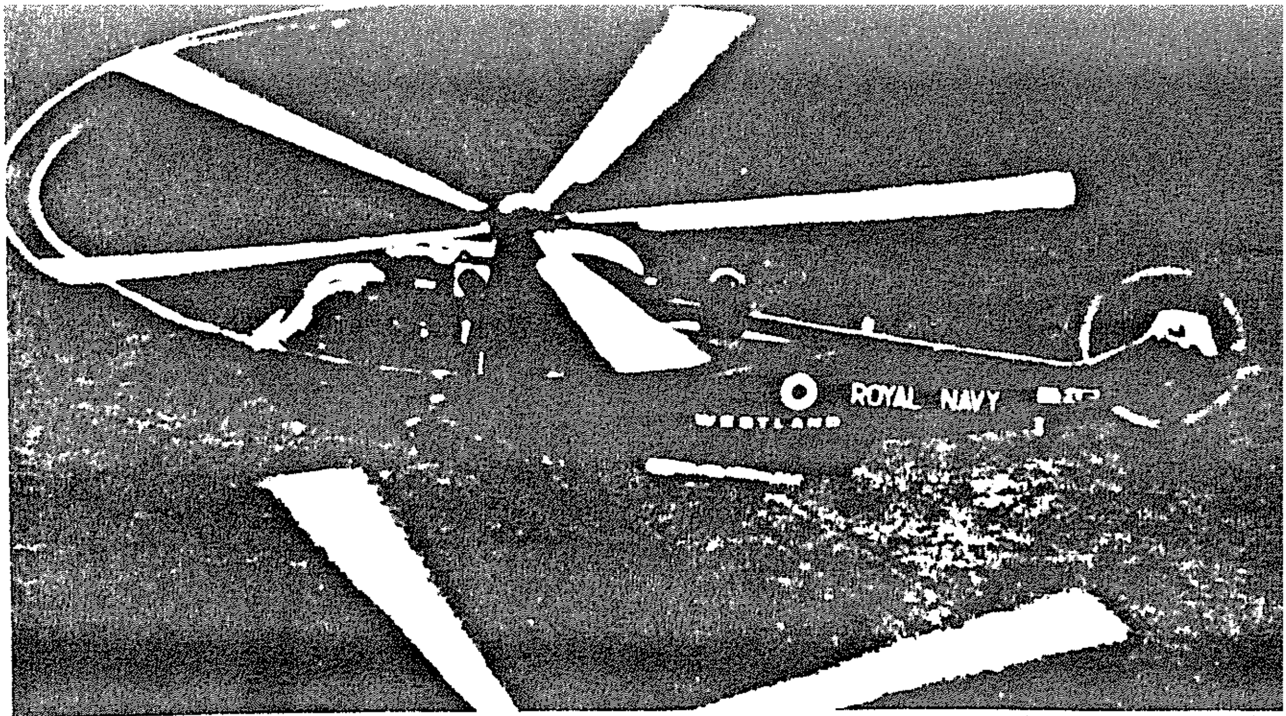
Fig. 1

Unfortunately the tip vortex strength, shape and position are currently hard to calculate accurately enough. It makes as well great problems to measure these characteristics just before the interaction with a blade. Therefore ,an interpretation of the measurements of the unsteady blade pressures is limited and it is difficult to obtain a better physical understanding of the BVI. An accurate computation of the unsteady blade pressures induced by the vortices is not possible.
In that situation a special test facility (s. figures 5 and 14) was designed to bring us a step foreward. A special delta wing in front of the rotor generates two concentrated leading edge vortices with a well known structure measured by a five hole probe. These vortices interact with a small two-bladed rotor.In a preliminary test phase an orientation of the rotor, shown in figure 5 ,was selected. Here the vortex axes are vertical to the rotor disk. In a second phase the rotor orientation was changed turning the vortex axis nearly parallel to the rotor disk. This orientation is similar to that of a helicopter during forward flight. The forward speed is simulated by the windtunnel flow.One of the delta vortices interacts with the rotor, the other passes downstream the rotor disk.

For the different vortex-rotor orientations the local velocity perturbations at the blades were calculated. Then ,the unsteady blade pressures and forces were computed by various theories (see chapter 2). The local pressure fluctuations were measured with Kulite transducers at various positions of the rotor blades. Measured and computed values are compared in the time-domain (see chapter 3).

2. Computation of the unsteady blade pressures and forces

Figure 2 illustrates the flow fluctuations for the case where the orientation of the vortex axis is normal to the rotor disk (according to figure 5). The flow distortions ,caused by the tangential velocity v_t of the vortex, are shown at three radial positions at the rotor blade.
The vortex induces a velocity component v in the rotor plane normal to the

leading edge of the blade. The component of the induced velocity parallel to the leading edge is neglected due to the low influence on the blade forces.

INFLOW DISTORTIONS DUE TO A TIP VORTEX

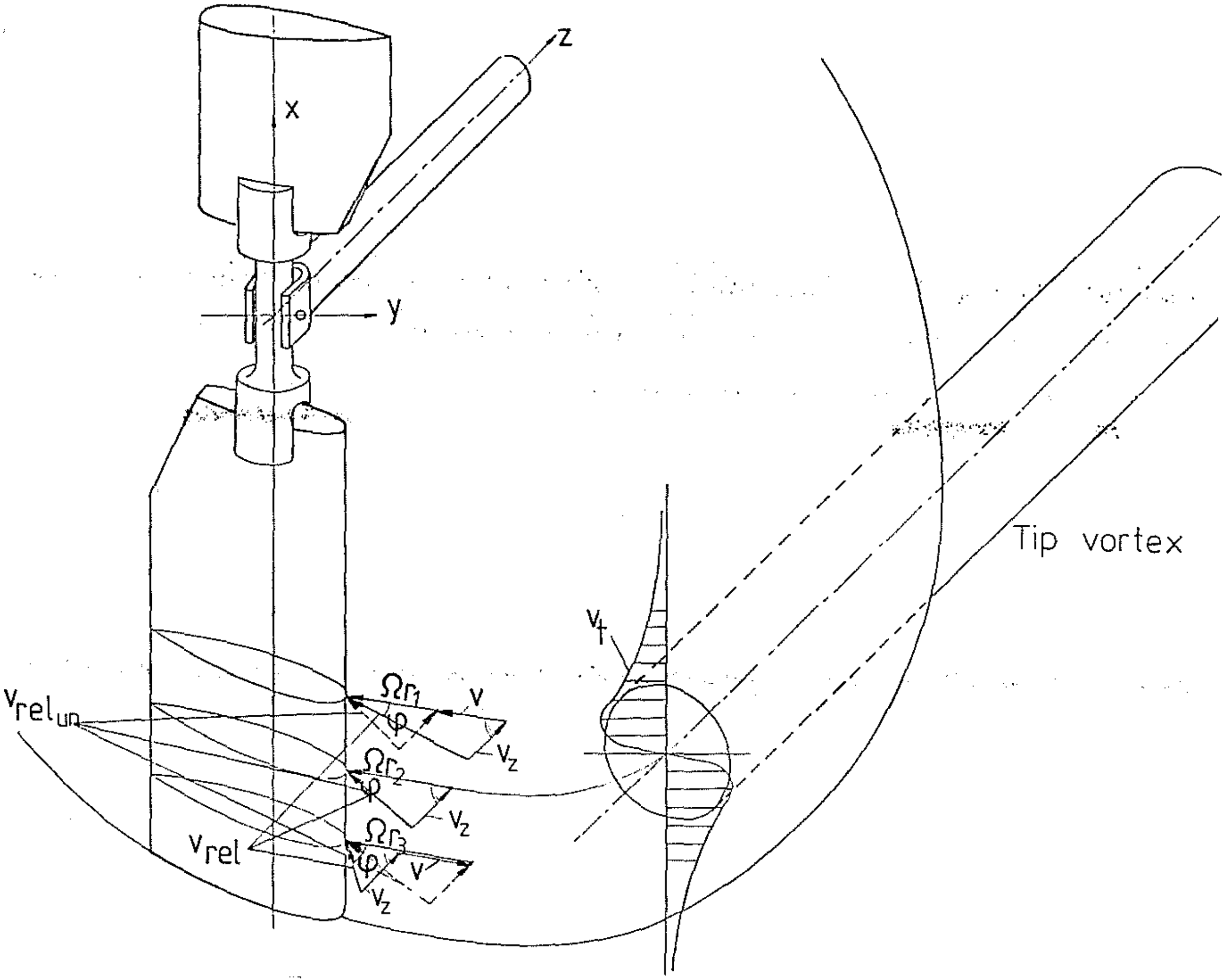

Fig. 2
In the figure Ωr is the blade velocity and v_z the axial velocity. The axial velocity distribution of the vortex is not shown. The figure reveals that both the direction and the magnitude of v_{rel} fluctuates. The general case of a vortex axis oblique to the rotor disk is shown in <u>figure 3.</u>

FLOW PERTURBATIONS AT A POINT Q CAUSED BY A TIP VORTEX

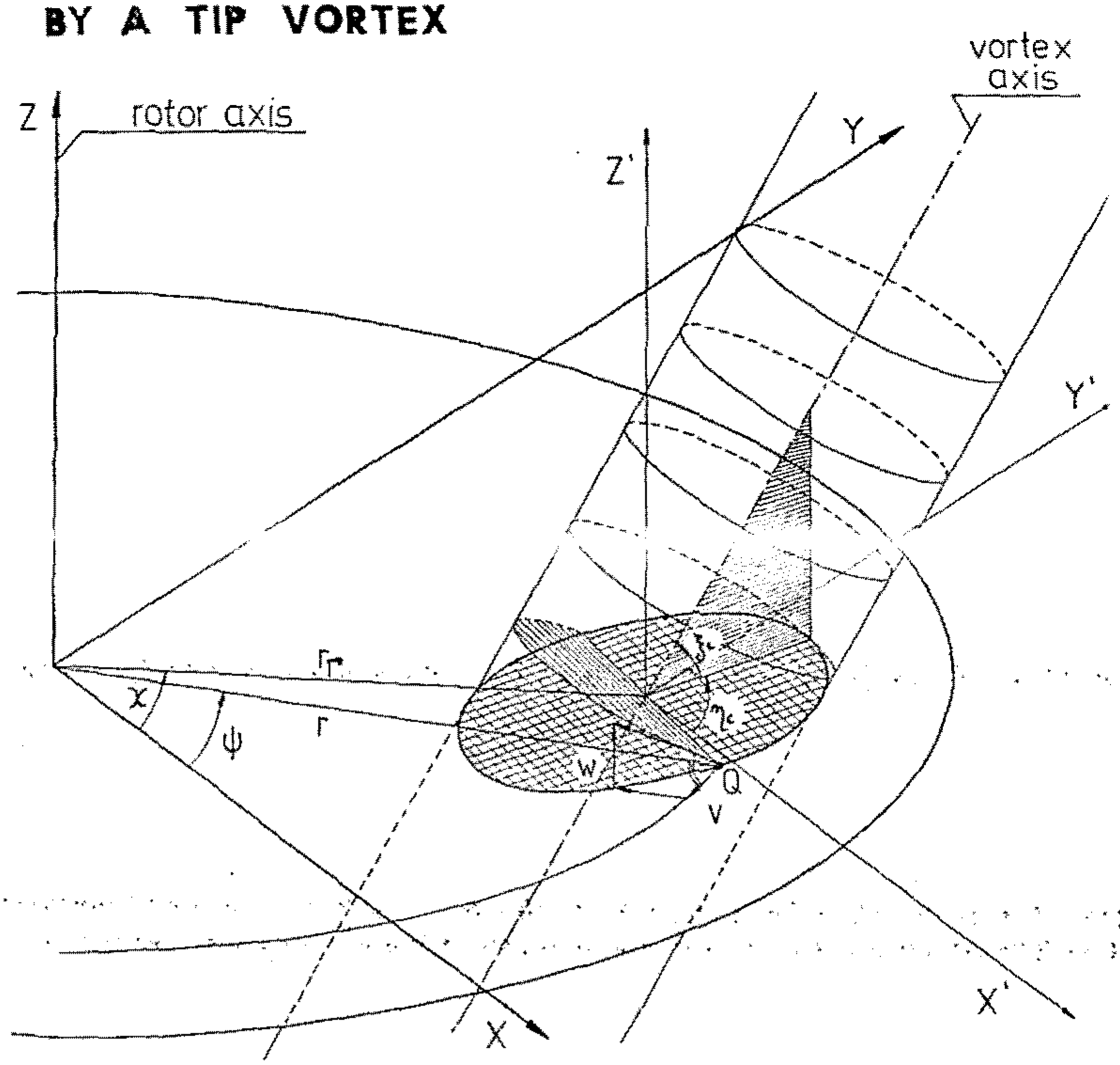

Fig. 3

The orientation of the vortex axis is given by the angles ξ_c and η_c where ξ_c is the angle between the rotor plane and the vortex axis and η_c is the angle between the projection of this axis into the rotor disk and the x-axis. At a point Q in the rotor plane a velocity is induced by the tangential velocity v_t of the vortex. Now, this induced velocity has now two components v and w, where w is normal to the rotor plane. The variations of the components v and w during one revolution can be computed for any blade element. The coordinate system x′ y′ z′ that is fixed on the blade elements. The axial velocities v_{ax} in the delta vorticies influence the components v and w and must be computed. For various radial positions the resultant fluctuations of v and w were Fourier analysed. The fluctuations of v and w are periodical and so the Fourier components have the disvrete frequencies $f_m = m\,b\,n$ ($m = 1, 2, 3, \ldots$), b being the number of rotor blades, n the rotor rotational speed and m the harmonic order.
These Fourier components are the input to the theories for computing the unsteady blade forces and pressures.

The applied theories neglect compressibility and friction effects and are based on singularity methods. An early contribution to the unsteady airfoil theory was made by KEMP and SEARS /2/ reducing the rotor to a two-dimensional plane blade row. The interference with neighbouring blades are ignored. The authors computed the unsteady lift of a flat plate only considering flow distortions normal to the plate. HORLOCK /3/ determined the lift fluctuations including distortions parallel to the undisturbed flow. Starting from these theories, NAUMANN and YEH /4/ developed the unsteady lift for a cambered airfoil that has angle of attack relative to the steady flow and velocity distortions normal and parallel to the chord. As shown in figure 4 the airfoil is represented by a vortex sheet arranged along the chord. The inflow can be represented by a mean velocity v_0 and the Fourier components of the flow disturbances.

DISTRIBUTION OF VORTICITY γ

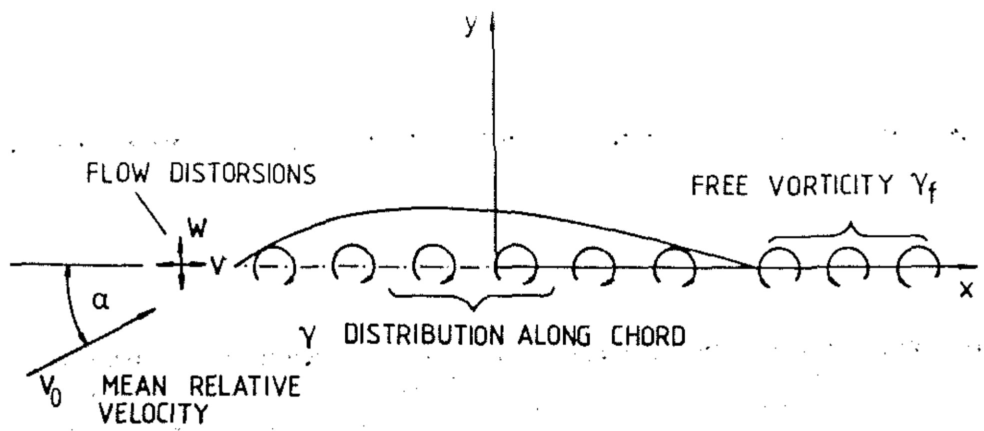

Fig. 4

Due to this inflow, the vorticity γ along the chord consists of a steady and a time dependent vorticity $\gamma = \gamma_s + \gamma_b$. Due to the variation of the bound vorticity (γ_b) free vortices (γ_f) will be shed. It is assumed that they are carried away with the mean velocity along a plane in the direction of the chord. The unsteady vorticities γ_b and γ_f induce unsteady velocities at the cambered airfoil. The total flow - mean flow plus disturbances plus total induced velocity - must be tangent to the camber line at all points. Using the known relation between γ_b and γ_f an interdependance between the flow disturbances v and w and the unsteady induced velocities can be developed. The result is an integral equation between γ_b and the known Fourier components of the flow disturbances v and w. Applying the Euler equation, the unsteady pressures harmonics $\tilde{p}_m(x,t)$ can be computed using the following equation:

$$\tilde{p}_{m_{p,s}}(x,t) = e^{i2\pi f_m t}\,\frac{\rho}{2}\left\{\pm\left(v_0\bar{\gamma}_{bm}(x) + \bar{v}_m(x)\,\gamma_s(x)\right) - \frac{1}{2}\gamma_s(x)\,\bar{\gamma}_{tm}(x)\right\}$$

Equations for computing the unsteady vorticity

$$\gamma_{tm} = \bar{\gamma}_{tm}\,e^{i2\pi f_m t} = (\bar{\gamma}_{bm} + \gamma_{fm})\,e^{i2\pi f_m t}$$

the unsteady bound vorticity

$$\gamma_{bm} = \bar{\gamma}_{bm} e^{i2\pi f_m t}$$

and the steady vorticity γ_s are deduced by SCHREIER /5/. The unsteady vorticities are influenced by the Fourier components of the flow distortions

$$v_m = \bar{v}_m e^{i2\pi f_m t}$$

and

$$w_m = \bar{w}_m e^{i2\pi f_m t}$$

The pressures on the suction side and on the pressure side of the blade have to be computed with (-) or (+) sign respectively. To compute the resultant unsteady pressure $\tilde{p}(x,t)$, the pressure harmonics $\tilde{p}_m(x,t)$ have to be superponed considering the phase relations resulting from the Fourier analysis of the flow distortions and from the computation of $\tilde{p}_m$. Then, the unsteady blade forces can be computed by integration of the pressures over the whole surface of the blades.

Additional to the method of NAUMANN and YEH a theory of HENDERSON /6/ can be applied to compute the unsteady blade forces. This theory additionally the interference effects of neighboring blades includes.

Furthermore, a three dimensional theory can be used for calculating the blade forces. This theory is based on the paper of FATHY /7/. The blades are allowed to be arbitrarily tapered and twisted. The reference blade is represented by a continuous distribution of vorticity while the other blades are replaced by concentrated radial lines of vortices. This theory was modified by KELLNER /8/ for including variable flow distortions at different radial positions. Furthermore, the influence of cambered leading and trailing edges can be calculated.

As shown by NEUWERTH /9/ the results of two and three dimensional theories show only small differences. To reduce the amount of computing time, the results in this paper are calculated by the theory of NAUMANN and YEH.

3. Theoretical and experimental results

3.1 Vortex axes normal to rotor disk

In a preliminary test phase an orientation of the rotor shown in figure 5 was selected - the vortex axes are vertical to the rotor disk. The geometry of the rotor blades is illustrated in figure 6. The blades have the symmetrical profile NACA 0012.

Six pressure transducers have been installed. The signals of the transducers 4 and 5 on the suction side are analysed below. Figure 7 shows the position of the two leading edge vortices relative to the rotor disk. The circle described by the pressure transducers 4 and 5 has a radius of 455 mm. The location of the vortex cores in the vertical position (y-axes) was varied.

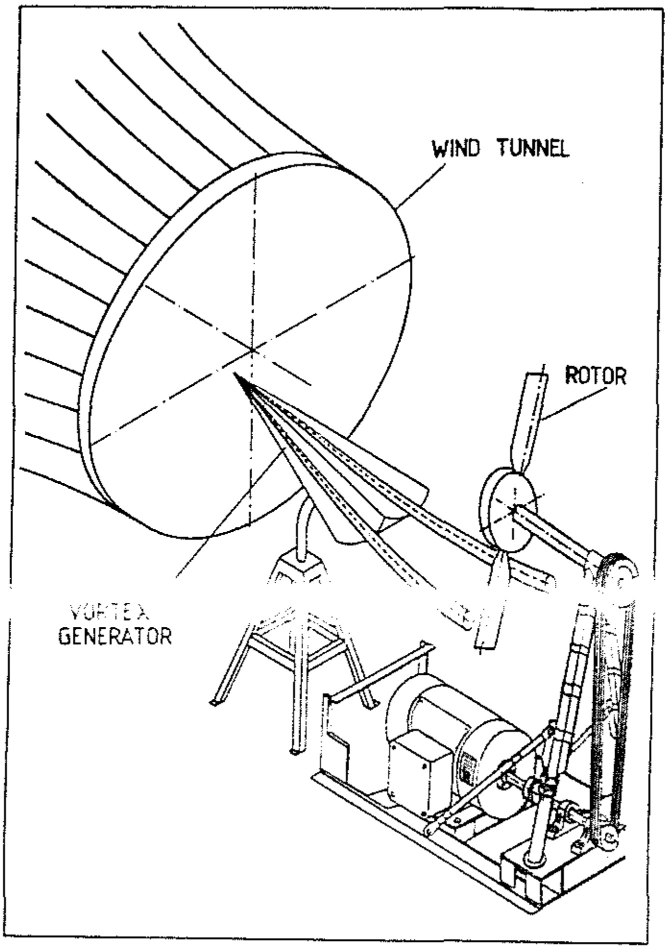

Fig. 5

GEOMETRY OF THE ROTOR BLADES

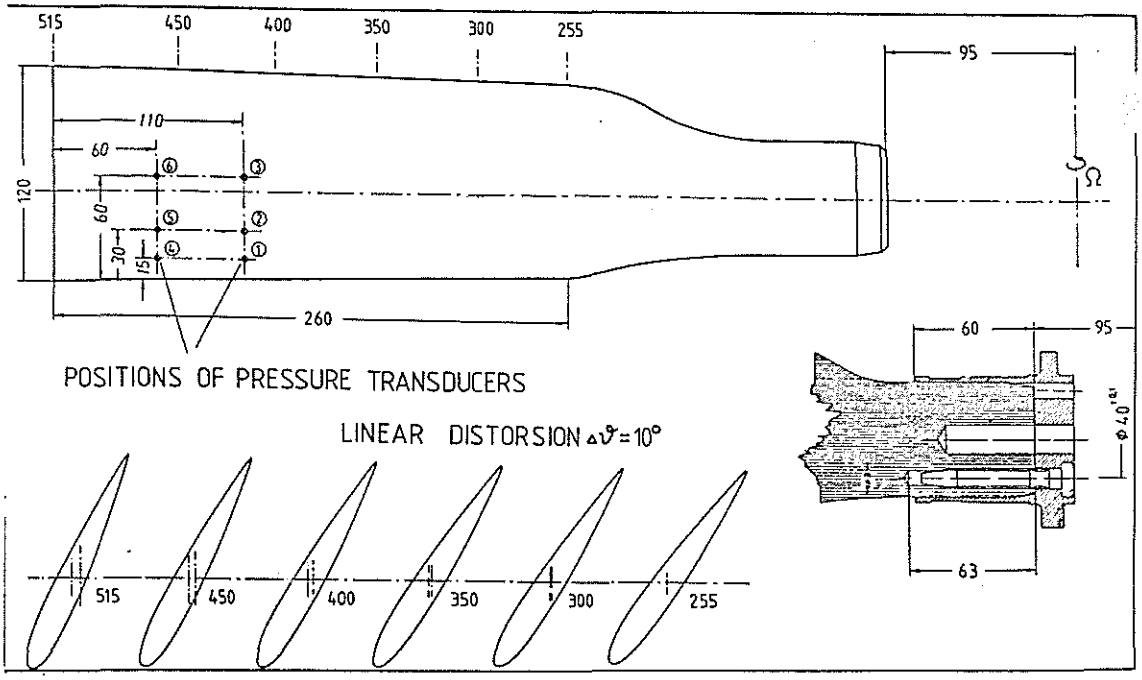

Fig. 6

GEOMETRY OF THE VORTEX-BLADE ARRANGEMENT

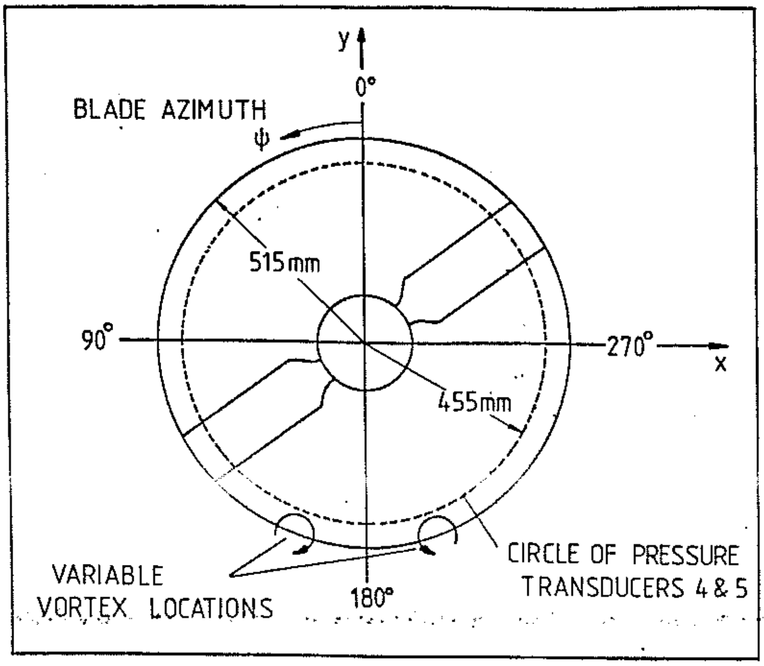

Fig. 7

The velocity distribution behind the delta wing was measured using a five hole probe. The axial speed v_{ax} and tangential speed v_t across the vortex cores are plotted in figure 8. Both components are related to the windtunnel speed v_{oo}.

Figure 9 demonstrates the pressure distribution in the vortex. In the core, the underpressure $p-p_{oo}$ has values of nearly seven times the dynamic pressure q_{oo} of the inflow.

A top view of the vortex path , visualized by smoke , is shown in figure 10. On the upper side of this figure the trailing edge of the delta wing and on the lower side the rotating rotor can be seen.

At this rotor orientation relative to the windtunnel the tip vortices of the rotor blades quickly travel downstream. Thus the induced velocities of the tip vortices in the rotor area being very small can be neglected. A result of this type of BVI is demonstrated in figure 11. The inflow has a speed of v_{oo} = 25 m/s. The rotational speed of the rotor is n = 2900 min^{-1}. The angle ϑ_t between the blade chord and them rotor area at the blade tip is 30°.

The upper plot in figure 11 shows the components v and w of the flow distorsions at the radial postition r = 455 mm of the pressure transducers 4 and 5 depending on azimuth. The position of the two vortex cores relative to the transducer path can be seen in the drawing right beside the plot.

The positions of the vortices relative to the rotor disk have been found out by means of flow visualisation with smoke. The flow distorsions have been calculated using figure 8.

VELOCITY DISTRIBUTION BEHIND THE VORTEX GENERATOR

(SECTION ACROSS THE TWO VORTEX - CORES)

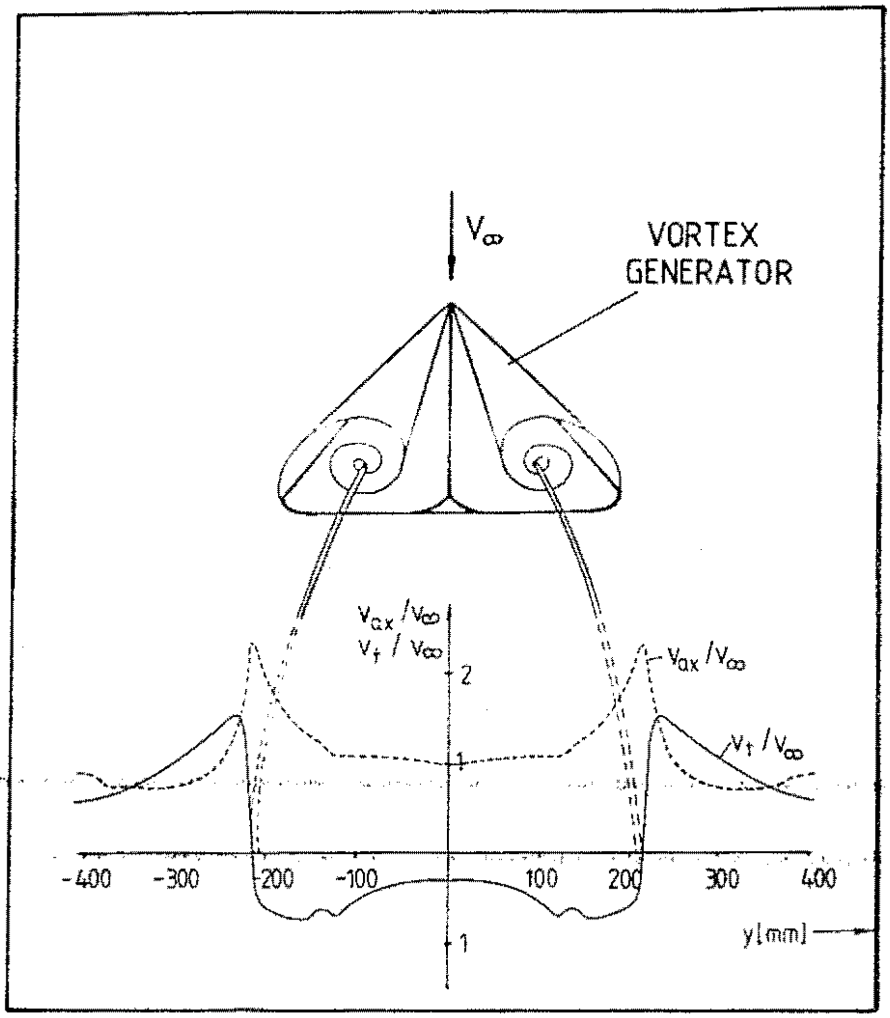

Fig. 8

PRESSURE DISTRIBUTION IN THE LEADING EDGE VORTEX

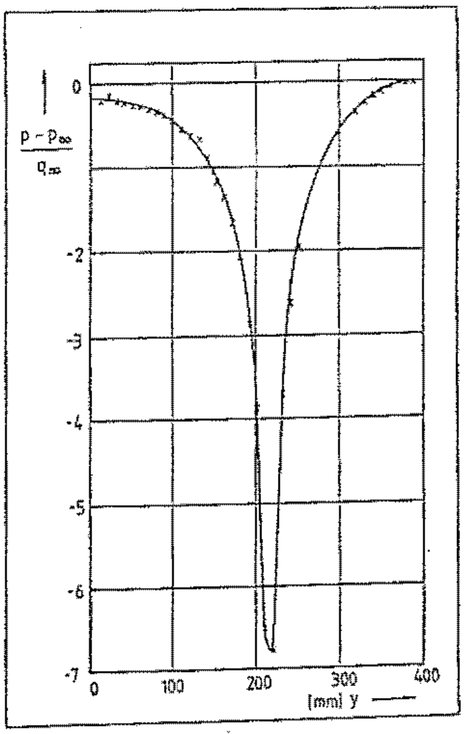

Fig. 9

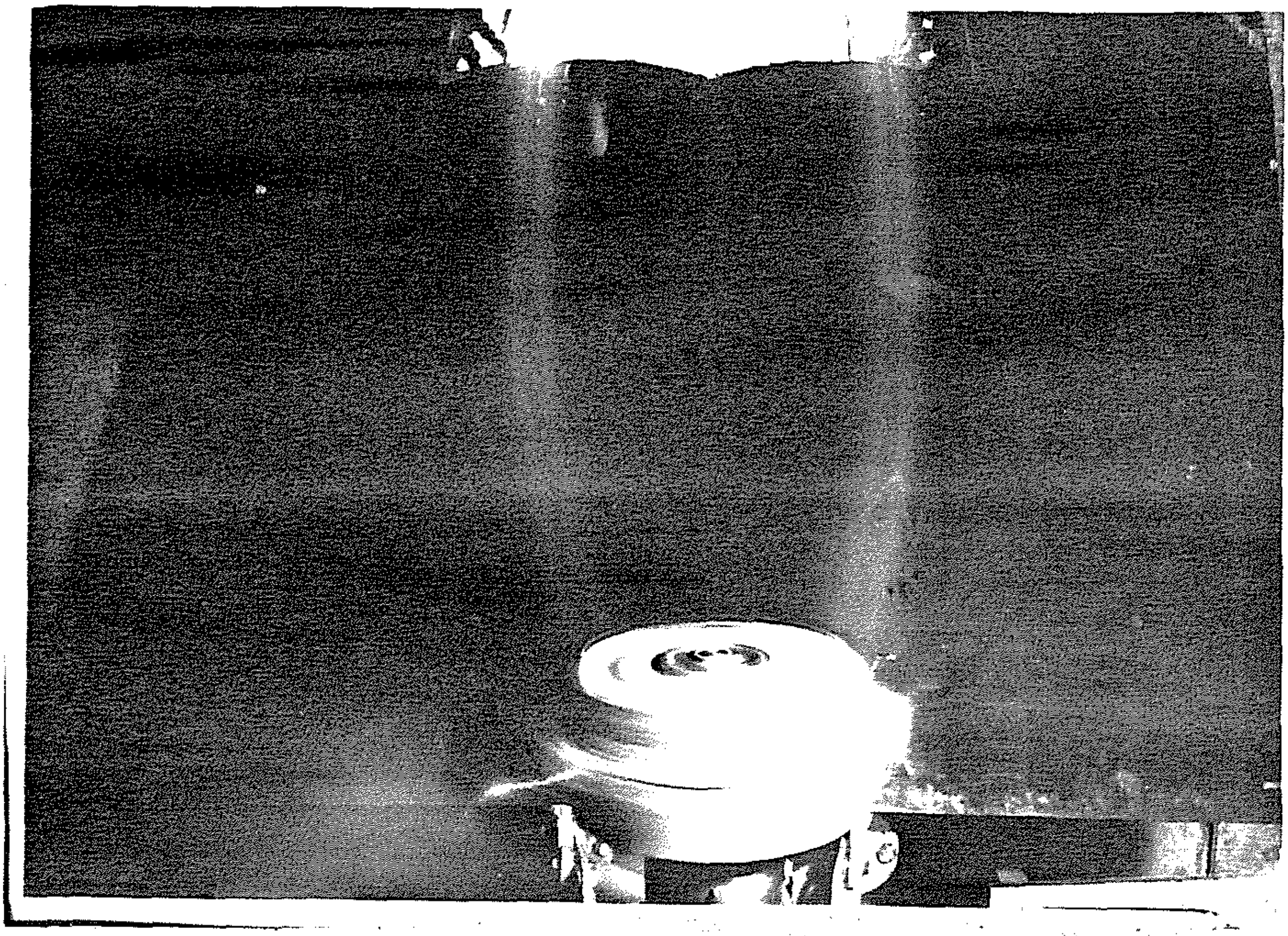

Fig. 10

The vortex at the blade azimuth $\psi = 164°$ diminishes the flow component v (v is negative) while the vortex at $\psi = 205°$ increases v.
At the radial position of transducer 4 and 5 the fluctuations of the component w, normal to the rotor area, are small due to the relatively large distances from the vortex cores (55 mm, respectively 85 mm). The two lower plots show the unsteady part $\tilde{p}$ of the pressure fluctuations on the suction side. The negative values of v(at $\psi = 164°$) reduce the local angle of attack and the stagnation pressure. Thereby the local underpressure is reduced, that means an increase of the pressure. The positive values of v(at $\psi = 205°$) has the contrary effect. Comparing the shape of the increased pressure fluctuations with the flow distorsions it can be concluded that the component v has a dominant influence. Because of the relatively large distances from the vortex cores the pressure distribution in the vortices has no significant influence on the unsteady pressure. The pressure fluctuations at the pressure transducer 4 (at 12.5 % blade chord) are higher than those at transducer 5 (at 25 % blade chord). This can be explained by the higher negative values of the steady $c_p = (p - p_{oo})/q_{oo}$ at the pressure transducer 4.

VELOCITY DISTORSIONS AND PRESSURE FLUCTUATIONS DUE TO TWO CONCENTRATED VORTICES WHOSE AXES ARE NORMAL TO ROTOR DISK

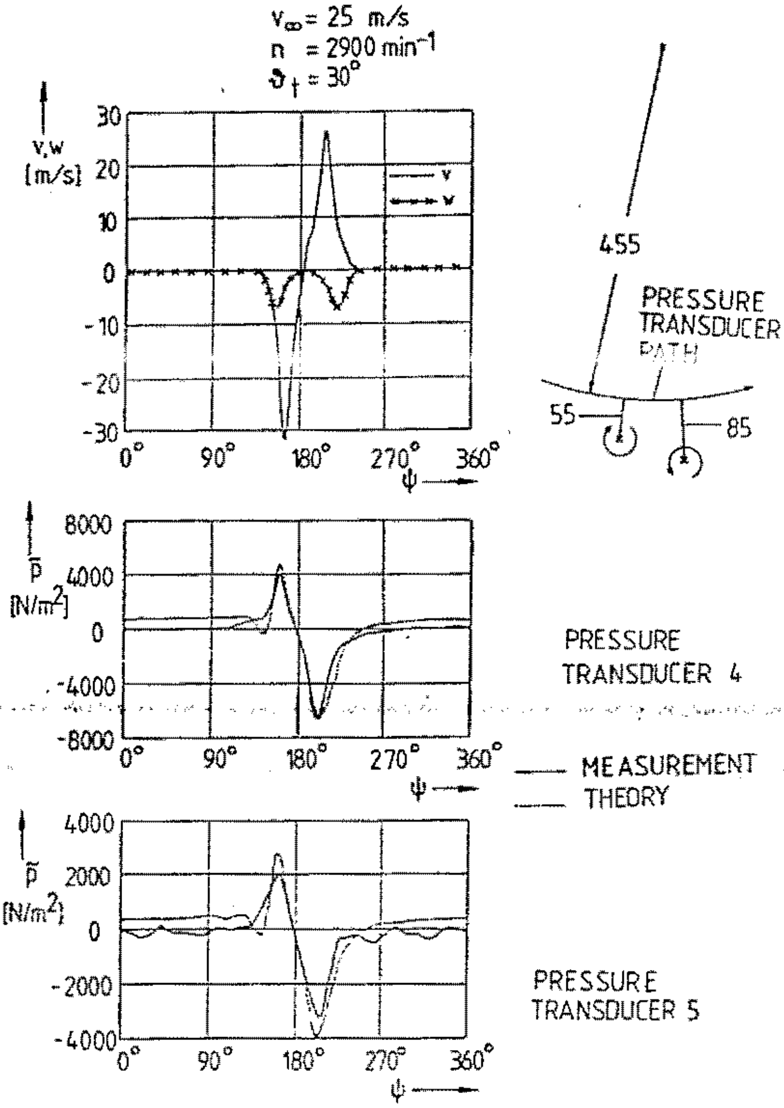

Fig. 11

The Fourier components of the fluctuations of v and w are input for the computation of the pressure fluctuations. A further input are the steady values of the effective angles of attack of the blades. These were computed by a program given in /10/ based on the 3-dimensional Goldstein theory. The unsteady pressures in figure 11, computed the 2-dimensional theory of Naumann and Yeh, show good agreement with the measurements. Only the extreme values at pressure transducer 5 are a little bit higher in the theory. A comparison of the shape of the measured and computed pressure fluctuations shows that Inflow separations due to BVI don't occur.
In figure 12 a case is shown where the vortex cores are closer to the path of the pressure transducer 4. The distances are 10 mm (vortes at $\psi = 160°$) and 25 mm (vortex at $\psi = 209°$).

VELOCITY DISTORSIONS AND PRESSURE FLUCTUATIONS DUE TO TWO CONCENTRATED VORTICES WHOSE AXES ARE NORMAL TO ROTOR DISK

v_∞ = 15 m/s
n = 2900 min^{-1}
ϑ_t = 22°

PRESSURE TRANSDUCER 4

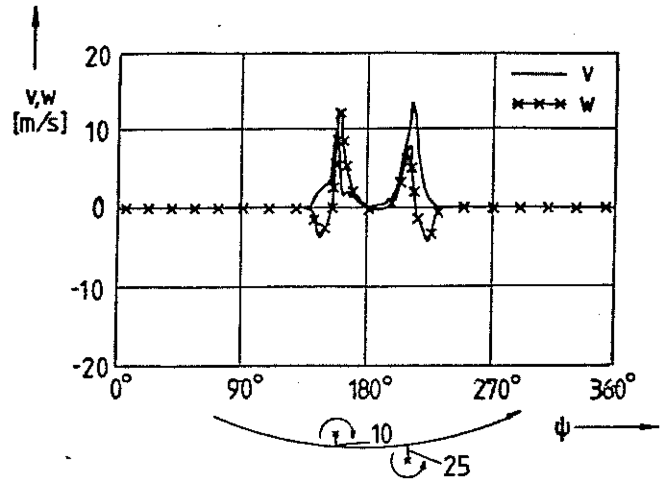

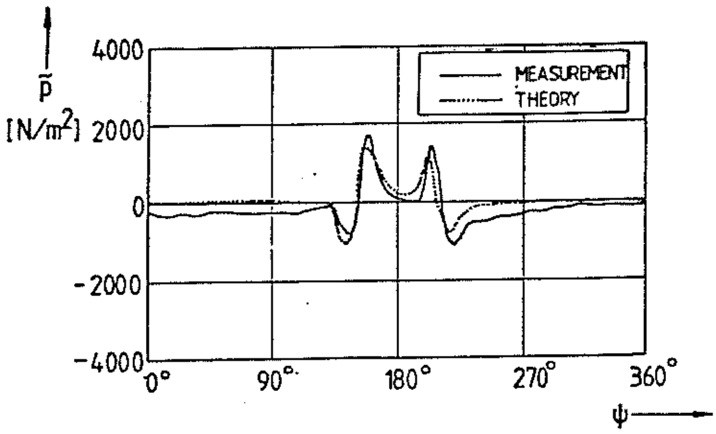

Fig. 12

Both vortices increase the flow component v .The axial velocity v_{ax} in the vortex cores (s. figure 8)increases w (w is positive). The increase of v leads to a decrease of the unsteady pressure $\tilde{p}$ at ψ= 160° and ψ= 209° .A similar influence is given by the underpressure in the vortex cores.However $\tilde{p}$ shows an increase at that angles. That means that the influence of the positive w is dominant: the local angles of attack are diminished, the underpressures at the section side are reduced and therefore the p-values are increased. Computed and measured unsteady pressures are in good agreement.

Figure 13 demonstrates that sound power spectrum ,generated by that type of BVI ,has a great number of harmonics with high sound power levels PWL.

That reveals the impulsive character of the radiated noise. The fundamental frequency is $f_1 = b\,n = 2 \cdot 2900/60 = 96.67$ Hz.

SOUND POWER SPECTRUM OF A ROTOR INTERACTING WITH TWO VORTICES WHOSE AXES ARE NORMAL TO ROTOR DISK

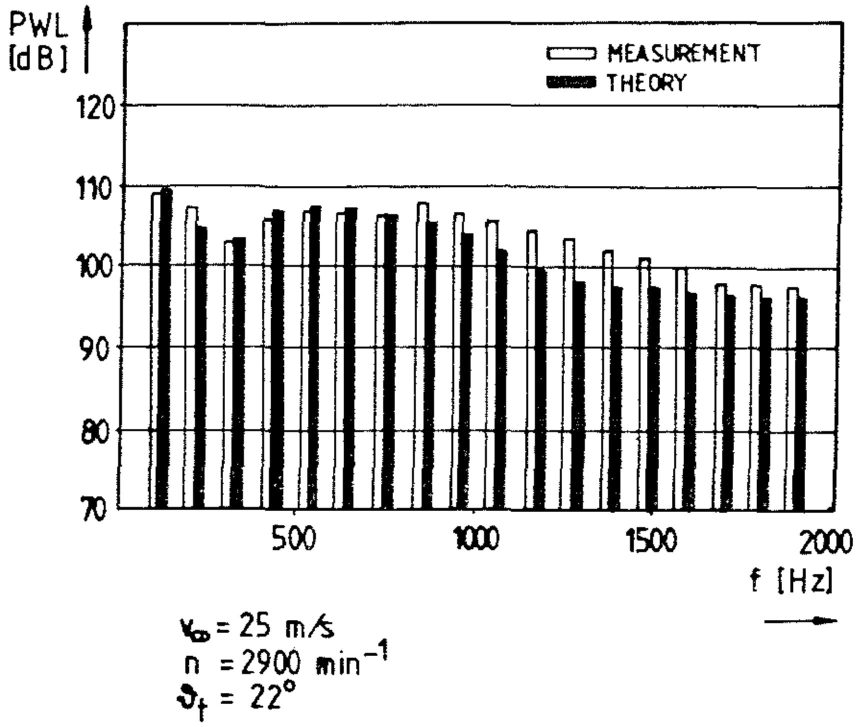

Fig. 13

To compute the sound power spectrum ,the rotor noise theories of Lowson /11/, Olberhead and Munch /12/ and Wright /13/ were extended by Schreier/5/. Inputs for this noise theory are the Fourier components and their phase relations of the computed unsteady blade forces. These inputs are strongly dependent on the radial position at the rotor; this influence is included in the noise theory.

3.2 Simulation of BVI for a helicopter during forward flight

Figure 14 demonstratesd the orientation of the rotor area. The vortex on the left side of the delta interacts with the rotor. The other vortex passes far downstream of the rotor, blown to the right by the outflow of the rotor, and thas has nearly no influence on the unsteady blade pressures. The angle between the rotor plane and the direction of the windtunnel flow is $\beta = -10°$. In that way the flow speed in the direction of the rotor axis is increased and the tip vortices generated by the rotor itself are quickly blown away from the rotor disk. So their influence on the blades is largely reduced.

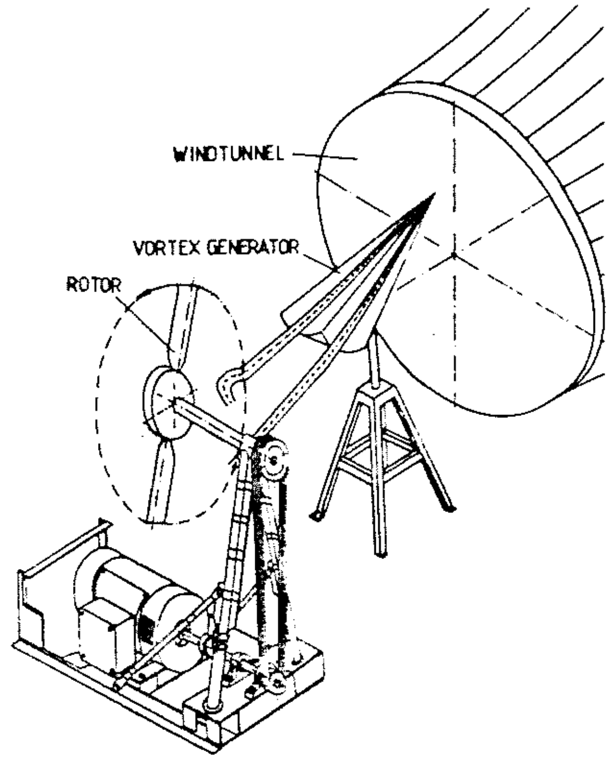

Fig. 14

Fig. 15

Subsequently a BVI with the following set of parameters is analyzed:
v_{oo} =20 m/s, n = 2700 min^{-1}, ψ_t= 10°, β = - 10°. A top view of that case is shown in figure 15.
On the upper part, the trailing edge of the vortex generator can be seen. The windtunnel flow v_{oo} enters the figure from above. The interacting vortex, visualized by smoke, is cut by the rotor blades. The path of that vortex axis in this horizontal area is plotted in figure 16. Also the angle β is illustrated.
Figures 17 and 18 show the path of the interacting vortex in the vertical area. Figure 17 demonstrates the instant of intersection while figure 18 is a snap shot a little bit later. The path of the vortex axis in this vertical area is plotted in figure 19. The radial position of the pressure transducer 4 (r = 455 mm) is far away from the intersection point of the vortex. The minimum distance between pressure transducer 4 and the vortex core are 77 mm. That means that at the radial position of that pressure transducer the flow *distortions are dominantly influenced by the tangential velocity v_t of the* vortex (s. figure 8).

PATH OF THE VORTEX AXIS IN THE HORIZONTAL AREA

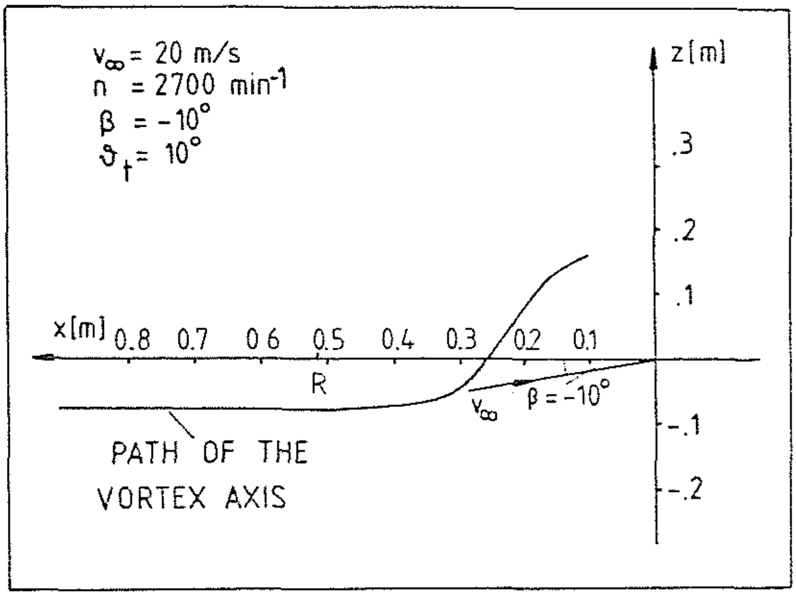

Fig. 16

Using the measured vortex path and the flow field in the leading edge vortex, the flow distortions v* and w* at the radial position of pressure transducer 4 are calculated (s. figure 20).
w* is equal to w plus the component of the windtunnel flow in the direction of the rotor axis. Due to the component of windtunnel flow parallel to the rotor area, the velocity component normal to the leading edge of the blades fluctuates with the amplitude v_{oo} cos β = 19,7 m/s in a harmonical way. These fluctuations are added to the flow distortions v caused by BVI. The orientation of the vortex core *relative to the blade element at the radial* position of pressure transducer 4 can be seen in the drawing at the right side for three values of blade azimuth ψ. At ψ= 250° v has its maximum and w is equal zero. At ψ = 240° the component w has a high negative and at ψ =260° a high positive value.

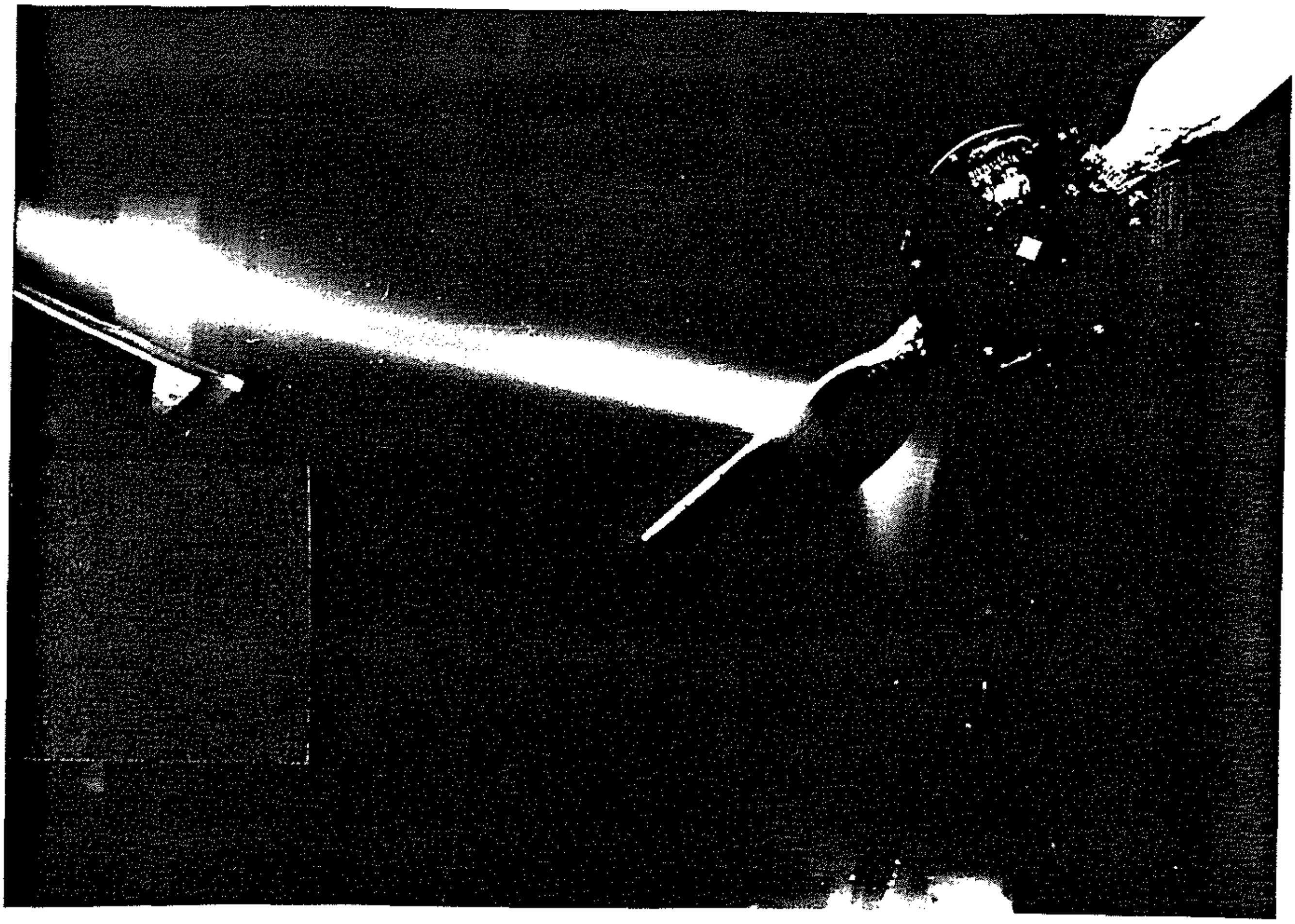

Fig. 17

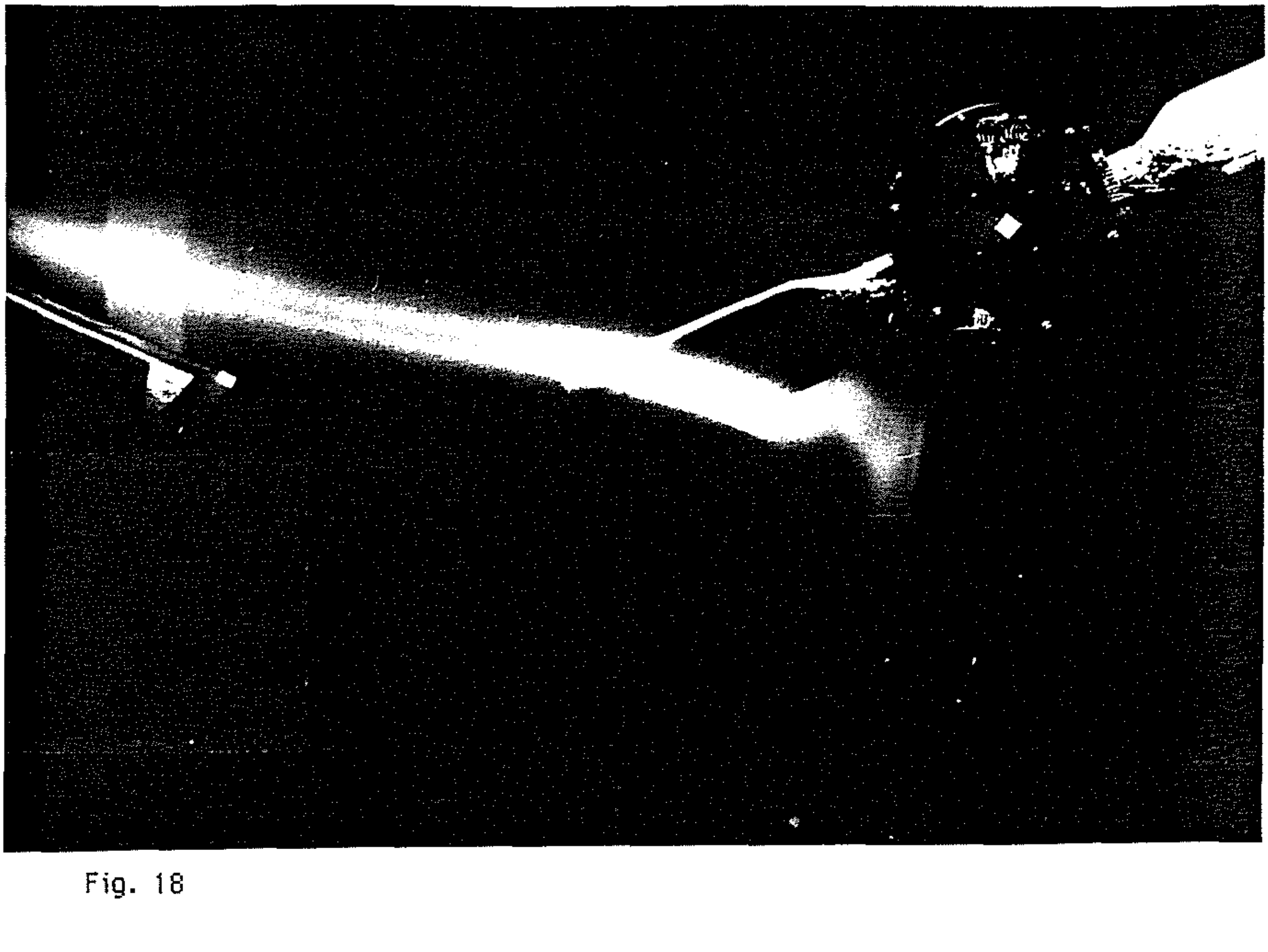

Fig. 18

PATH OF THE VORTEX AXIS IN THE VERTICAL AREA

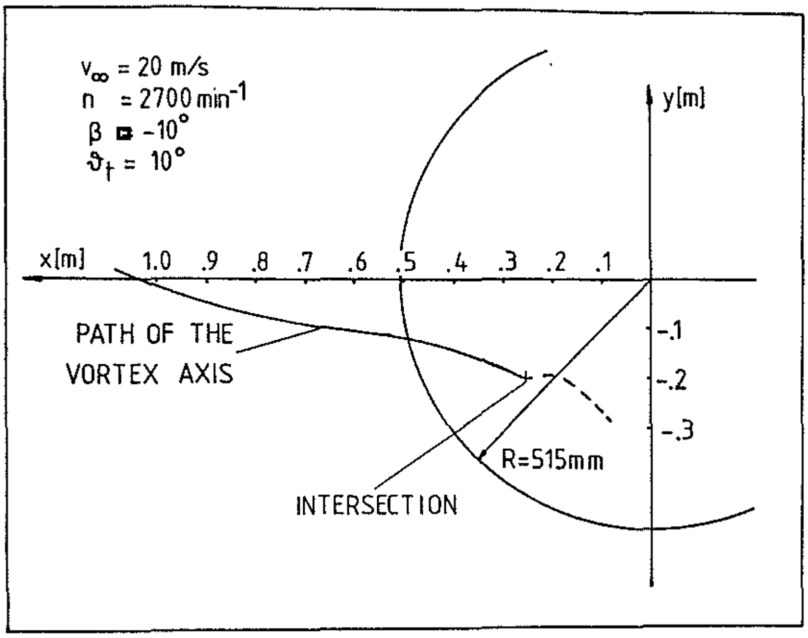

Fig. 19

FLOW DISTORSIONS AT THE RADIAL POSITION OF PRESSURE TRANSDUCER 4

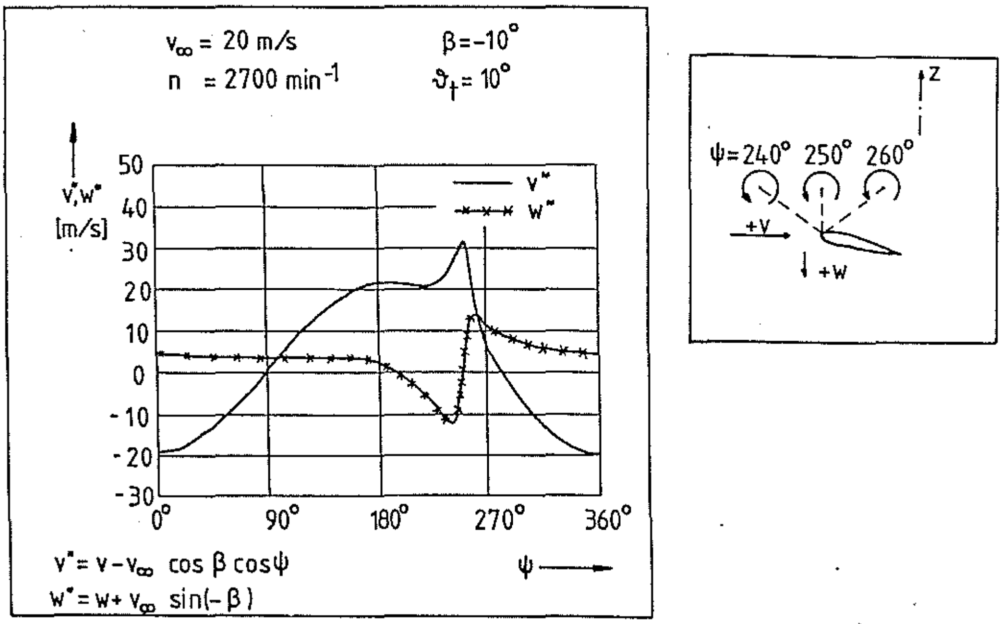

Fig. 20

PRESSURE FLUCTUATIONS

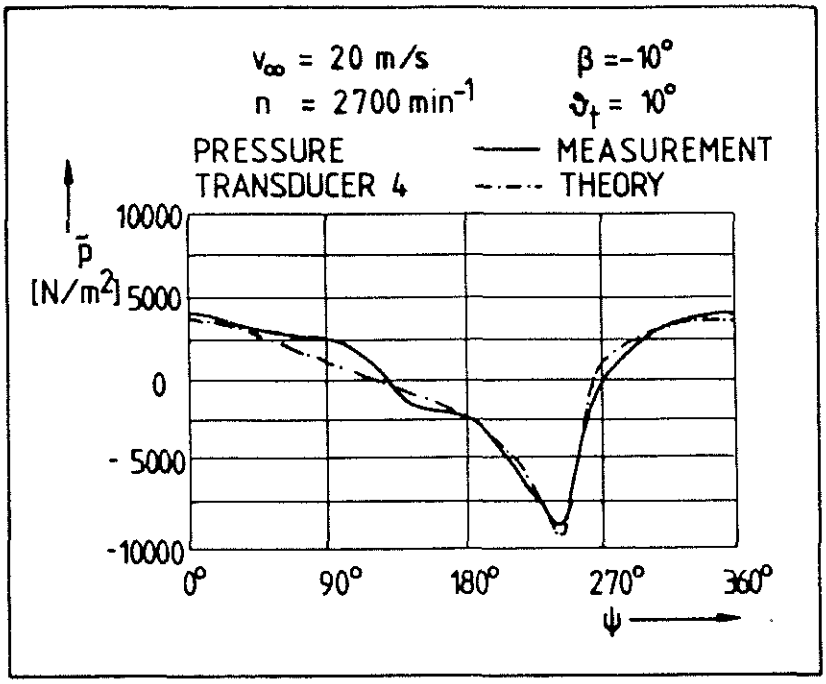

Fig. 21

The unsteady pressure $\tilde{p}$ at transducer 4 (s. figure 21) shows a fluctuation *due to the component of windtunnel flow parallel to the rotor area. These* fluctuations are superimposed by those effected by the vortex. The negative values of w in the region of ψ= 240° increase the angles of attack and leads to a growing of the underpressure at the suction side. The shape of $\tilde{p}$ in that region has an impulsive character. The computed values of $\tilde{p}$ (theory of NAUMANN and YEH) are in good agreement with the measured ones. The small discrepances between ψ= 90° and ψ= 180° can be interpreted as the influence of the tip vortices of the rotor itself. These interactions are under the way to be analysed in more detail.

4. Conclusions

During certain flight conditions the vortices shed from the tips of helicopter rotor blades pass near the operating rotor disk or are cut by the blades. Unfortunately the tip vortex strength, shape and position are currently hard to predict accurately or to measure just before interaction with the blades. In thes paper a basic understanding of this BVI-mechanism was tried to achieve by using a special test arrangement. In this case, vortices were generated by a delta wing located in front of a small test rotor. The structure of these vortices was measured by a five hole probe. The position of these vortices before and during the interaction with a two bladed rotor was detected by applying smoke visualisation.

The vortices induce flow distortions whose components were calculated for various radial blade elements as a function of the blade azimuth. These

flow distortions are the input to theories applied in this paper for computing local unsteady blade pressures and unsteady blade forces. The local unsteady pressures are measured with small pressure transducers and show , for the analysed rotor tip Mach numbers $M_t \leq 0.52$, good agreement with the computed values.
Depending on the different orientations of the interacting vortex relative to the rotor, the unsteady blade pressures were investigated. Flow separations due to BVI were not observed.
The pressure fluctuations show an impulsive character. That is demonstrated by the high number of harmonics in the noise spectrum and by the subjective loudness. A noise theory was extended to the application of the noise radiation due to BVI and their results are in quite good agreement with the measured noise levels.

5. References

/1/ D. A. BOXWELL, F. H. SCHMITZ, Full-Scale Measurements of Blade-Vortex Interaction Noise, Journal of the American Helicopter Society, Oct. 1982.

/2/ N. H. KEMP, W. R. SEARS, The unsteady Forces Due to Viscous Wakes in Turbomachines, Journal Aeron. Sci. Vol. 22, pp. 478-483, 1955.

/3/ J. H. HORLOCK, Fluctuating Lift Forces on Airfoils Moving through Transverse Chordwise Gusts, Journ. Basic Engineering, Vol. 90 Ser. D. Nr. 4, pp. 494-500, 1968.

/4/ H. NAUMANN, H. YEH, Lift on Pressure Fluctuations of a Cambered Airfoil under Periodic Gusts and Applications in Turbomaschinery, Paper 72-GT-30, ASME, 1972.

/5/ J. SCHREIER, Experimentelle und theoresche Untersuchungen der Schallabstrahlung von Rotoren und Propellern, die sich in Wirbel Wirbelfeldern bewegen, Dissertation RWTH Aachen, 1983.

/6/ R. E. HENDERSON, The Unsteady Response of an Axial Flow Turbomachine to an Upstream Disturbance, Ph. D. Thesis, NTIS, AD-759029, 1972.

/7/ A. F. A. FATHY, The Unsteady Circulation Distribution in Rotors and its Application to Noise Studies, Ph.D.- Thesis, South Dakota State Univ., 1973

/8/ A. KELLNER, Experimentelle und theoretische Untersuchungen über den Einfluß inhomogener Geschwindigkeitsverteilung in der Zuströmung auf die Lärmerzeugung von Mantelschrauben, Diss. RWTH Aachen, 1980.

/9/ G. NEUWERTH, et al., Fluctuating Forces and Rotor Noise due to Distorted Inflow, ICAS-Proceedings pp. 674-688, 13. ICAS-Congress, Seattle, USA, 1982.

/10/MBB- VFW, Propellerrechenverfahren-Programm POPAG, 1975.

/11/ M. V. LOWSON, Theoretical Studies of Compressor Noise, NASA CR-1287, 1969.

/12/ I. B. OLLERHEAD, C. L. MUNCH, An Application of Theory to Axial Compressor Noise, NASA CR-1519, 1970.

/13/ S. E. WRIGHT, Discrete Radiation from Rotating Periodic Sources, Journ. Sound. Vibr., Vol. 17, pp. 437-498, 1971.